JOURNAL OF VIROLOGY, Nov. 2006, p. 10989–10999 Vol. 80, No. 22
0022-538X/06/$08.00+0 doi:10.1128/JVI.01154-06

Acid Sphingomyelinase Deficiency Increases Susceptibility to Fatal Alphavirus Encephalomyelitis▽

Ching G. Ng and Diane E. Griffin*

W. Harry Feinstone Department of Molecular Microbiology and Immunology, Johns Hopkins Bloomberg School of Public Health, Baltimore, Maryland 21205

Received 3 June 2006/Accepted 23 August 2006

Sindbis virus (SV), an enveloped virus with a single-stranded, plus-sense RNA genome, is the prototype alphavirus in the *Togaviridae* family. In mice, SV infects neurons and can cause apoptosis of immature neurons. Sphingomyelin (SM) is the most prevalent cellular sphingolipid, is particularly abundant in the nervous systems of mammals, and is required for alphavirus fusion and entry. The level of SM is tightly regulated by sphingomyelinases. A defect in acid sphingomyelinase (ASMase) results in SM storage and subsequent intracellular accumulation of SM. To better understand the role of the SM pathway in SV pathogenesis, we have characterized SV infection of transgenic mice deficient in the ASMase gene. ASMase knockout (ASM-KO) mice were more susceptible to SV infection than wild-type (WT) or heterozygous (Het) animals. Titers of SV were higher in the brains of ASM-KO mice than in the brains of WT mice. More SV RNA was detected by in situ hybridization, more SV protein was detected by immunohistochemistry, and more terminal deoxynucleotidyltransferase-mediated dUTP-biotin nick end labeling-positive cells were present in the cortex and hippocampus of ASM-KO mice than in those of WT or Het mice. Interleukin-6 (IL-6), but not IL-1β or tumor necrosis factor alpha, was elevated in infected ASM-KO mice compared to levels in WT or Het mice, but studies with IL-6-KO mice and recombinant SV expressing IL-6 showed no role for IL-6 in fatal disease. Together these data indicate that the increase in susceptibility of ASM-KO mice to SV infection was the result of more-rapid replication and spread of SV in the nervous system and increased neuronal death.

Sindbis virus (SV), an enveloped virus with a single-stranded, plus-sense RNA genome, is the prototype alphavirus in the *Togaviridae* family (60). In nature, SV cycles between mosquito and avian vertebrate hosts, producing a lifelong infection in mosquitoes and transient infection in vertebrates. In humans, SV infection can cause fever, rash, and arthritis. In mice, SV causes encephalomyelitis, and neurons in the brain and spinal cord are the primary target cells. The severity of infection in mammals depends on both virus and host factors (20, 32) and makes SV an excellent model to study the pathogenesis of virus-induced encephalomyelitis.

Cellular lipids play an important role in several aspects of alphavirus replication, but the roles of specific lipids and their interactions with cellular proteins are not clear (22, 53, 56). The plasma membranes of eukaryotic cells consist primarily of sphingolipids, glycerophospholipids, and cholesterol (16). Sphingomyelin (SM), comprised of a highly hydrophobic ceramide moiety and a hydrophilic phosphorylcholine head group, is the most prevalent cellular sphingolipid, is particularly abundant in the nervous system, and is often associated with cholesterol (16, 50). Hydrogen bonds and hydrophobic interactions mediate tight interactions between the cholesterol sterol ring system and the ceramide moiety of SM (16, 50, 54). The lateral association of sphingolipids is further promoted by hydrophilic interactions between the sphingolipid head groups. The association of these lipids and high local concentrations result in their separation from phospholipids within the bilayer and the transformation of these sphingolipid- and cholesterol-rich membrane domains into a distinct liquid ordered phase (i.e., lipid rafts) (50, 54).

Both cholesterol and sphingolipids are essential for the fusion of the envelope of SV with the cellular membrane to initiate virus infection (39, 56, 66). Cholesterol is also important for budding of SV from the host cell (30, 31, 35). RNA synthesis takes place on the cytoplasmic surfaces of intracellular membranes derived from endosomes and lysosomes while the synthesis of envelope proteins occurs at the rough endoplasmic reticulum (RER) (22). Changes in the lipid makeup of these membrane-bound organelles could affect the rate and efficiency of replication of SV.

The level of sphingolipids present in eukaryotic cells is tightly regulated by sphingomyelinases (SMases, or sphingomyelin phosphodiesterases; EC 3.1.4.12) (33, 55, 58), which cleave the phosphodiester bond between ceramide and phosphorylcholine of SM (28). SMases are classified into acid, neutral, and alkaline sphingomyelinases (ASMases, NSMases, and Alk-SMases, respectively) by their pH optima. Lysosomal ASMase (pH optimum, 4.5 to 5.0) and NSMase (pH optimum, 7.0 to 7.8) are well characterized (17, 28, 43).

Human and murine ASMases (UniGene nomenclature, SMPD1) are the product of single genes, although differences in oligosaccharide structure and N-terminal proteolytic processing allow for the generation of multiple isoforms (33). In humans, an inherited deficiency of ASMase activity results in Niemann-Pick disease (NPD). Type A NPD (NPD-A) is a severe neurodegenerative disorder that leads to death by 3 years of age, while patients with type B NPD have little or no

* Corresponding author. Mailing address: W. Harry Feinstone Department of Molecular Microbiology and Immunology, Johns Hopkins Bloomberg School of Public Health, 615 North Wolfe Street, Baltimore, MD 21205. Phone: (410) 955-3459. Fax: (410) 955-0105. E-mail: dgriffin@jhsph.edu.

▽ Published ahead of print on 30 August 2006.

neurologic involvement and often survive into adulthood (17). Homozygous ASMase knockout (ASM-KO) mice appear normal at birth and develop normally until about 4 months of age, when they begin to show signs of neurologic disease, including ataxia, tremors, and loss of appetite (17, 43). In ASM-KO mice, as in humans with NPD-A, there is no detectable ASMase activity. This results in an increase in the level of SM in the brain, kidney, lung, bone marrow, and liver (17, 41, 43). In addition to the intracellular SM accumulation, the levels of other lipids, such as cholesterol, lysobisphosphatidic acid, and glycosphingolipids, are elevated in patients with NPD-A (28).

Although several NSMase activities have been described for different mammalian tissues and cell lines, the most prominent, plasma membrane-bound, Mg^{2+}-dependent NSMase activity is found mainly in the brain and, to a lesser extent, in other tissues (28, 33, 43, 58). Recently, two Mg^{2+}-dependent mammalian NSMases (SMPD2 and SMPD3) have been identified and characterized (15, 59, 62, 68). The SMPD2- and SMPD3-deficient double mutant transgenic mice completely lack NSMase activity and have a life span of about 2 years (59). Unlike ASM-KO mice, these NSMase-deficient mice do not develop an SM storage disease, indicating that SM turnover is primarily due to ASMase activity (59). The third family of SMases, Alk-SMases (pH optimum, 8.5), is found in the intestinal mucosa and bile (7, 40). Alk-SMase does not appear to participate in signal transduction (7, 24, 40).

Metabolites derived from sphingolipids by the action of SMases constitute a novel class of cellular signaling molecules involved in apoptosis, cell proliferation, and differentiation (13, 51). A variety of stimuli have been implicated in inducing the intracellular production of ceramide, and some of these molecules include tumor necrosis factor alpha (TNF-α), interleukin-1 (IL-1), Fas ligands, nerve growth factor, and ionizing radiation (13, 25). Alterations of host cell sphingolipid metabolism have profound effects on the replication and pathogenesis of many pathogens. Inhibition of SMase by synthetic ceramide *N*-palmitoyl-DL-dihydrosphingosine interferes substantially with replication of herpes simplex type 1 virus (57). Yields of infectious herpes virus from ASMase-deficient fibroblasts are lower than those from normal fibroblasts (57). In vitro, genetic deficiency or pharmacological inhibition of ASMase blocks cellular uptake of rhinoviruses and *Pseudomonas aeruginosa* (10, 11). Infection with a neuroadapted strain of SV leads to an elevation of ASMase and NSMase activities, an increase in intracellular ceramide levels, and apoptosis (18). Mice deficient in the ASMase gene are highly susceptible to infection with *Listeria monocytogenes* and *Salmonella enterica* serovar Typhimurium (64). Thus, SM is important for the outcome of infection with both bacterial and viral pathogens.

To determine the roles of the SM pathway in the pathogenesis of SV and test the hypothesis that ASMase is an important determinant of SV-induced neuronal apoptosis, we have characterized SV infection of mice deficient in the ASMase gene, a major regulator of SM metabolism (33, 58). ASM-KO mice were more susceptible to SV infection, and this was associated with enhanced replication and spread of SV in the central nervous system (CNS) and increased death of neurons.

MATERIALS AND METHODS

Cells and virus. BHK-21 cells were grown in Dulbecco's modified Eagle medium (Gibco BRL, Gaithersburg, MD) supplemented with 10% fetal bovine serum, 100 U/ml of penicillin, and 100 μg/ml of streptomycin. The TE strain of SV was grown and assayed by plaque formation in BHK cells (32).

Mice. ASM-KO mice on a C57BL/6 background were bred from heterozygous (Het) animals (17). The heterozygous animals were obtained from Memorial Sloan-Kettering Cancer Center (courtesy of Richard Kolesnick). The mouse ASMase gene is made up of six exons spanning ~4.5 kb. To disrupt the ASMase gene, a PGK*neo* expression cassette (where PGK is phosphoglycerate kinase) was inserted into exon 2 in the reverse orientation relative to the ASMase coding sequence. Mice were genotyped using modifications of a previously published protocol (17). Two sets of primers were used: ASMase sense (Ps, 5′-GCC GTG TCC TCT TCC TTA C-3′) and antisense (PA1, 5′-CGA GAC TGT TGC CAG ACA TC-3′) from exon 2 of the ASMase gene flanking the PGKneo cassette and PGKneo primers (Neo5, 5′-GGA GAG GCT ATT CGG CTA TG-3′, and Neo3, 5′-GCT CTT CAG CAA TAT CAC GG-3′) in the PGK*neo* expression cassette. C57BL/6 and IL-6 knockout (IL-6-KO) mice on a C57BL/6J background (Jackson nomenclature, $Il6^{tm1Kopf}$) were purchased from The Jackson Laboratory (Bar Harbor, Maine) (26). The mice were bred and raised in the Johns Hopkins University pathogen-free animal facilities in microisolator cages. All animal studies had the approval of and followed the guidelines of the Johns Hopkins University Animal Care and Use Committee.

Mice were infected at 8 days of age by intracranial inoculation of the right hemisphere of the brain with 1,000 PFU SV. At various times after infection, mice were anesthetized and perfused with phosphate-buffered saline (PBS). For virus titration, brains and spinal cords were separately homogenized in PBS and the virus assayed by plaque formation on BHK-21 cells. For histology, the left hemisphere of the brain was fixed with 4% paraformaldehyde and embedded in paraffin.

ASMase and NSMase assays. ASMase and NSMase activities were measured according to previously described methods, with minor modifications (14, 49). Briefly, to measure ASMase activity, 50 μg of protein was incubated for 60 min at 37°C in a buffer (200 μl final volume) containing 0.2 M sodium acetate (pH 5.5), 0.1 M $MgCl_2$, and 0.25 mg/ml of human serum albumin for ASMase or 0.2 M Tris-HCl (pH 7.4) for NSMase and 1 μl of [N-*methyl*-^{14}C]SM (25 μCi/ml, specific activity of 55.0 mCi/mmol; Amersham Biosciences Corp., Piscataway, NJ). Radioactive phosphorylcholine produced from [^{14}C]SM was extracted with 1 ml of chloroform:methanol (2:1, vol/vol) and 200 μl of distilled water. [^{14}C]phosphorylcholine was measured by scintillation counting of 200 μl of the upper aqueous phase extracted from each sample.

Hippocampal slice cultures. Organotypic slice cultures of the hippocampus were prepared from 5-day-old wild-type (WT), Het, and ASM-KO mouse pups as previously described (65). Slices were cultured for 8 days and then infected with SV (2×10^6 PFU in 100 μl) by slow drip. Supernatant fluids were collected at various times for virus assay. At 72 h postinfection, slice cultures were stained for 5 h with 1 μg/ml propidium iodide (PI) (Sigma, St. Louis, MO) to determine cell viability. Fluorescence was measured by computer-based image analysis. Cell death units were calculated for each genotype by use of the following formula: cell death unit = (average time of exposure of mock-infected slice cultures/average time of exposure of SV-infected slice cultures). The results are presented as the averages of four slice cultures per genotype.

In situ hybridization. Nucleotides 8638 through 8912 (E2 coding region) were amplified by PCR from the 633 DNA and cloned into the pGEM-3Z vector (Promega). Digoxigenin (DIG)-labeled RNA probes were made by in vitro transcription with DIG-UTP (Roche Diagnostics, Indianapolis, IN) from the SP6 promoter after plasmid linearization with EcoRI (61). DIG-labeled RNA probes were then purified using mini-Quick Spin columns (Roche Diagnostics) according to the manufacturer's recommendations.

In situ hybridization was performed as previously described, with minor modifications (47, 61). Briefly, sections from paraffin-embedded tissues were deparaffinized, hydrated, rinsed in distilled water, refixed with 4% paraformaldehyde for 20 min, treated with 200 mM HCl for 15 min, treated with 0.25% acetic anhydride in 0.1 M Tris (pH 8.0) for 10 min, washed in Tris-buffered saline (TBS), digested with 20 μg of proteinase K (Roche Diagnostics) for 20 min at 37°C, and then incubated in TBS at 4°C to stop the proteinase K digestion. The sections were then dehydrated, incubated in chloroform for 20 min, rehydrated, and incubated in 2× SSC (1× SSC is 0.225 M NaCl plus 0.0225 M sodium citrate) for 5 min. For prehybridization, each section was incubated with 50 μl of hybridization solution (2× SSC, 10% dextran sulfate, 1 μg/ml sheared herring sperm DNA, 0.02% sodium dodecyl sulfate, 50% formamide) at 56°C for 1 h. DIG-labeled probes were diluted 1/50 in hybridization buffer, and 50 μl of the diluted

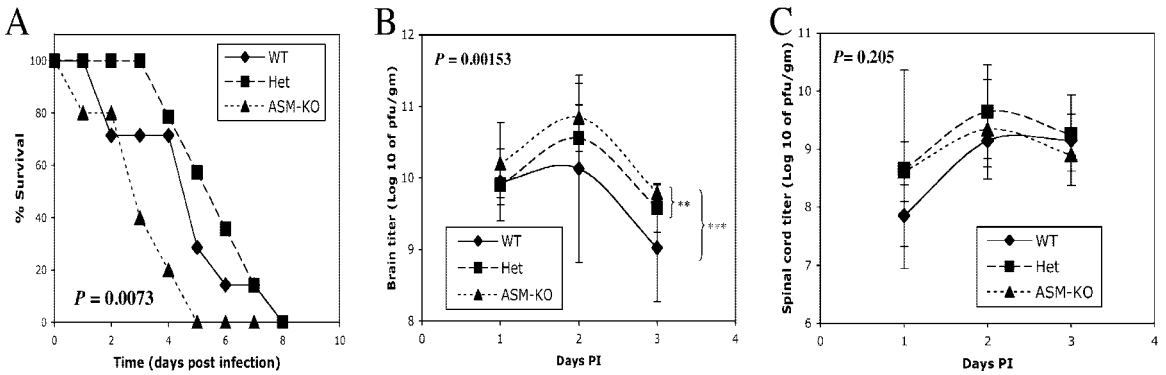

FIG. 1. Mouse survival and virus replication in the CNS. (A) Eight-day-old WT ($n = 7$), heterozygous ($n = 14$), and ASM-KO ($n = 5$) mice were intracranially infected with 1,000 PFU of SV and monitored for survival. ASM-KO mice died more rapidly after infection than WT and Het mice ($P = 0.0073$, Kaplan-Meier survival analysis, log rank test). Virus replication in the brains (B) and spinal cords (C) was assessed 1 to 3 days postinfection by plaque assay. Each point represents the geometric mean ± standard deviation of ≥4 mice (**, $P < 0.005$; ***, $P < 0.001$; two-way ANOVA).

probe was added to each section. The sections were then covered with a coverslip, heated to 95°C for 4 min, and hybridized overnight at 56°C. Unbound probe was removed by washing sections with 2× SSC followed by incubating them in 1× SSC-50% formamide at 56°C for 1 h.

For detection, sections were rinsed in 1× SSC, blocked in Roche Diagnostics blocking buffer for 30 min at room temperature (RT), incubated with alkaline phosphatase-labeled anti-DIG antibodies (Roche Diagnostics) at a 1/500 dilution in blocking buffer for 1 h at RT, and washed five times with TBS. Fast Red substrate in 0.1 M Tris (pH 8.2) was used for color development, and slides were mounted in Permount.

Immunohistochemistry. Immunohistochemistry was performed using an avidin-biotinylated enzyme complex method (23) with modifications. Paraffin sections were first dewaxed and rehydrated by standard methods and treated with 1% H_2O_2 in methanol at RT for 30 min to permeabilize and block endogenous peroxidase activity. The sections were then boiled in deionized water for 30 s, washed with PBS, and blocked with blocking buffer (0.5% nonfat dried and 1% normal goat serum in PBS) for 1 h. Sections were further incubated with rabbit anti-SV immunoglobulin G (1:50) in blocking buffer overnight at 4°C. After being washed with PBS, sections were incubated with biotinylated goat anti-rabbit immunoglobulin G (1:100; Vector Laboratories, Burlingame, CA) for 1 h at RT. Immunolabeled cells were stained with a VECTASTAIN standard ABC kit (Vector Laboratories) and 3,3′-diaminobenzidine tetrachloride (Polysciences, Inc., Warrington, PA) according to the manufacturer's protocol. Sections were then dehydrated, rinsed in Histo-Clear (National Diagnostics, Atlanta, GA), and mounted in Permount.

Terminal deoxynucleotidyltransferase-mediated dUTP-biotin nick end labeling (TUNEL) staining was done according to the manufacturer's recommendation (Roche Diagnostics). Dewaxed and rehydrated sections were treated with 20 μg/ml of proteinase K in 10 mM Tris-HCl (pH 7.4) for 30 min at 37°C, rinsed with PBS, and permeabilized (0.1% Triton X-100, 0.1% sodium citrate in PBS) for 8 min at RT. Sections were incubated with 50 μl of labeling solution at 37°C for 1 h in a humidified chamber. The reaction was terminated by rinsing the slides three times with PBS, and sections were incubated with sheep antifluorescein antibody conjugated with alkaline phosphatase for 30 min at 37°C and visualized by a Vector Blue alkaline phosphatase substrate kit (Vector Laboratories). Sections were then dehydrated, rinsed in Histo-Clear, and mounted in Permount.

EIA. Brain and spinal cord samples collected at various times postinfection were homogenized in PBS and centrifuged for 15 min (300 × *g*) at 4°C (48). The samples at each time point were then pooled for each genotype ($n \geq 4$ for each time point), and the levels of IL-1β, TNF-α, and IL-6 were determined using mouse IL-1β, TNF-α, and IL-6 enzyme immunoassay (EIA) kits (BioSource, Camarillo, CA) according to the manufacturer's recommendations. Total protein in each sample for each time point was determined by the Bradford method (1) to calculate the level of each cytokine per mg of protein.

Construction of recombinant SV encoding the murine IL-6 gene. Murine IL-6 (mIL-6) was cloned from mRNA extracted from B6 mouse brain. Briefly, brain was homogenized in RNA STAT-60 (RNAzol reagent; Tel-Test, Friendswood, TX) and total RNA was isolated with a standard chloroform extraction protocol and precipitated with isopropanol. The RNA was resuspended in diethyl pyrocarbonate water, and the mIL-6 gene was amplified by PCR using the following primers: forward primer 5′-GCG CGG TCAC CAT GAA GTT CCT CTC TGC A-3′ and reverse primer 5′-GCG CGG TGA CCC TAG GTT TGC CGA GTA GA-3′. The PCR product was subcloned into the TOPO cloning vector (Invitrogen, Carlsbad, CA), digested with BstEII, and gel purified, and the 663-bp mIL-6 open reading frame was ligated into the BstEII site of the double subgenomic SV vector (dsTE) in forward orientation. mIL-6 in reverse orientation was cloned into dsTE with the following primers: forward primer 5′-GCG CGG TGA CCA TGA AGT TCC TCT CTG CA-3′ and reverse primer 5′-GCG CGG TCA CCC TAG GTT TGC CGA GTA GA-3′. The dsTE plasmid containing the mIL-6 gene was linearized with XhoI and transcribed in vitro using SP6 RNA polymerase. Stocks of recombinant viruses were generated by transfecting the full-length RNA into BHK-21 cells and collecting the supernatant fluid when more than 70% cytopathic effect was observed. Virus titers were determined by plaque assay on BHK-21 cells.

Statistical analysis. Differences in mouse mortality were determined by Kaplan-Meier survival analysis using Stat View (SAS Institute, Inc., Cary, NC) and a log rank test with 2 degrees of freedom. Student's *t* test and analysis of variance (ANOVA) were performed using R (GNU project).

RESULTS

Mice deficient in the ASMase gene (ASM-KO mice) are more susceptible to SV-induced fatal encephalitis. To determine whether endogenous ASMase has a role in the pathogenesis of SV-induced fatal encephalitis, ASM-KO, C57BL/6 (WT), and Het mice were studied (17). Mice were infected with SV at 8 days of age, before neurologic disease due to accumulation of SM in the CNS occurs in ASM-KO mice. SV caused 100% mortality in all groups (Fig. 1A). However, the mean day of death was day 3.2 for ASM-KO mice, day 4.7 for WT mice, and day 5.9 for Het mice, indicating an increased susceptibility of ASM-KO mice to SV-induced death ($P = 0.0073$, Kaplan-Meier survival analysis, log rank test). No difference in survival was detected between WT and Het mice ($P = 0.3843$).

Virus replication in brain and spinal cord. To determine if more-rapid death was associated with increased virus replication, brains and spinal cords of infected mice were collected and assayed for virus 1 to 3 days after infection (Fig. 1B and C). In brain, ASM-KO mice had the highest titers at each time point ($P = 0.00153$, two-way ANOVA) (Fig. 1B). The brain titers of ASM-KO mice were also higher than those of WT ($P = 0.005$, two-way ANOVA) and Het ($P = 0.0009$, two-way

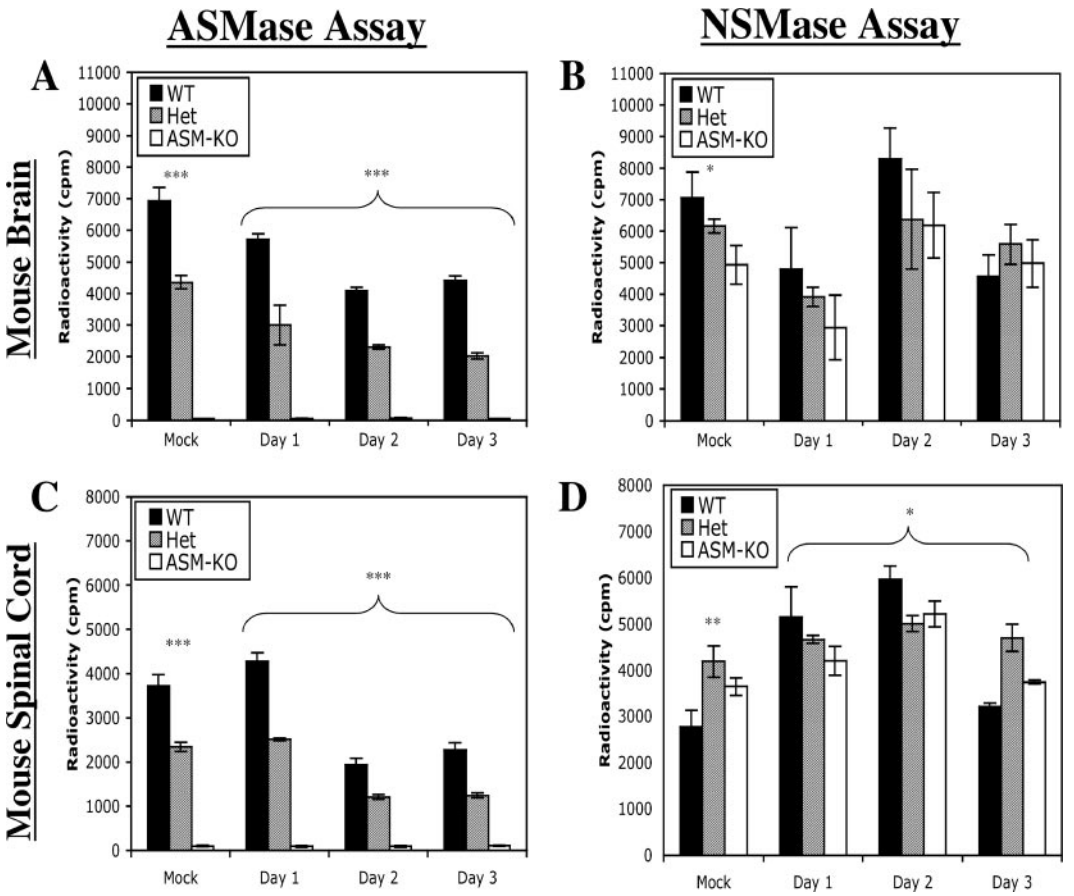

FIG. 2. Levels of ASMase and NSMase activities in brain and spinal cord. ASMase (A and C) and NSMase (B and D) activities were assayed in the brains (A and B) and spinal cords (C and D) of mock- and SV-infected mice. Samples from infected mice were pooled ($n \geq 4$ for each time point), and the geometric means ± standard deviations of three replicates are shown (*, $P < 0.05$; **, $P < 0.005$; ***, $P < 0.001$; ANOVA).

ANOVA) mice individually. WT and Het brain titers were not different ($P = 0.209$, two-way ANOVA) (Fig. 1C). In spinal cord, there were no significant differences in titers between the groups ($P = 0.205$, two-way ANOVA). Peak viral titers were on day 2 postinfection in the brains and spinal cords for all three genotypes of mice.

ASMase and NSMase assays. To confirm the phenotypes of the mice and to determine the effect of virus infection on SMase activity in the brains and spinal cords, ASMase and NSMase activities were measured (Fig. 2). Brain and spinal cord samples collected from WT mice 1 day after infection had high levels of ASMase activities, those from Het mice had intermediate levels, and those from ASM-KO mice had no detectable ASMase activity ($P < 0.001$, ANOVA) (Fig. 2A and C). After SV infection, ASMase activity decreased in the brains of WT and Het mice. Activity in the brain was 62.3% of that of the mock-infected samples in WT mice and 46.5% in Het mice 3 days after infection (Fig. 2A). Significant differences in the levels of ASMase activity among the three genotypes of mice persisted ($P < 0.001$, two-way ANOVA) (Fig. 2A). In the spinal cord, ASMase activity decreased for both WT and Het animals 2 and 3 days after infection (Fig. 2C). At day 3 after infection, ASMase activity in the spinal cord decreased to 61.2% of levels of the mock-infected mice in WT mice and 53.0% in Het mice (Fig. 2C). No ASMase activity was detected in brains or spinal cords of ASM-KO animals (Fig. 2C).

NSMase activity was measured to determine whether compensatory changes occurred. Mock-infected WT mice had the highest levels of NSMase activity in the brain, followed by Het and ASM-KO animals ($P = 0.0129$, ANOVA) (Fig. 2B), as has been observed by others (17, 43). The three genotypes of mice followed similar patterns after SV infection, with no significant difference in the levels of NSMase activity in the brain for the first 3 days of infection ($P = 0.0674$, two-way ANOVA) (Fig. 2B). In spinal cords from mock-infected mice, the levels of NSMase activity were different, with higher levels in the Het mice ($P = 0.0035$, ANOVA) (Fig. 2D). After SV infection, there was generally an increase in the levels of NSMase activity in the spinal cord for the first 2 days, with the highest levels in WT mice ($P < 0.01749$, two-way ANOVA) (Fig. 2D). For both brain and spinal cord samples, the peak NSMase level corresponded with the peak viral titer at day 2 postinfection (Fig. 1B and C).

Virus replication and cell death in SV-infected hippocampal slice cultures. To investigate the effect of the loss of ASMase activity on SV infection of mouse neurons, hippocampal tissue slices were prepared from 5-day-old mice and infected with

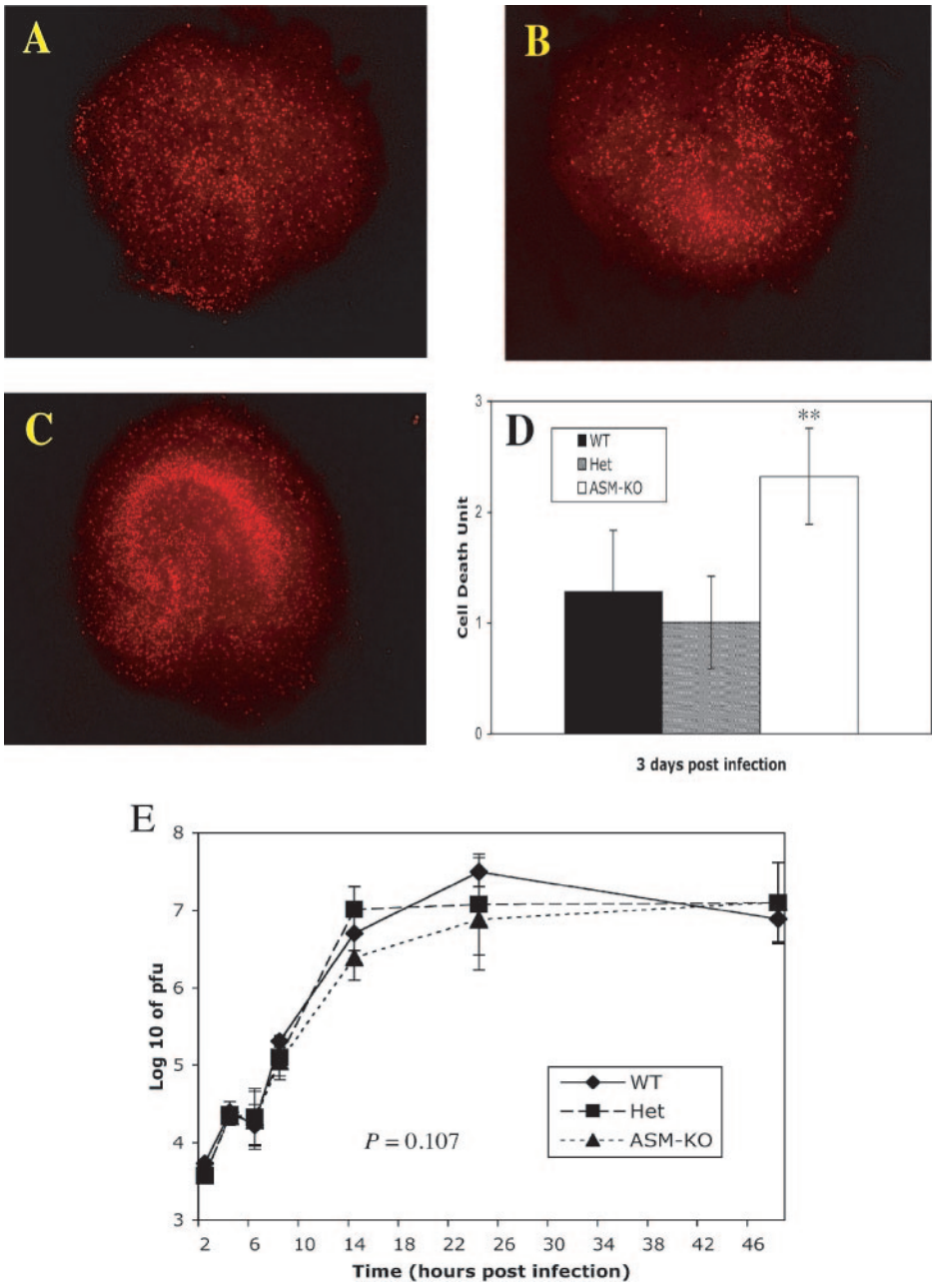

FIG. 3. Cell death and virus replication in hippocampal slice cultures. Hippocampal slices from 5-day-old WT (A), Het (B), and ASM-KO (C) mice were cultured for 8 days and then infected with 2×10^6 PFU of SV. Slices were stained with 1 μg/ml PI 3 days postinfection to assess neuronal death. Cell death units (average time of exposure of mock-infected slice cultures/average time of exposure of SV-infected slice cultures) were determined for each genotype ($n = 4$) (D). More cell death was present in ASM-KO hippocampal slice cultures than in those for WT or Het mice (**, $P < 0.01$). (E) Growth curve of SV in the hippocampal slice cultures. Each point is the geometric mean ± standard deviation of two cultures (four hippocampal slices per culture).

SV. After 3 days of infection, neuronal death was determined by staining the tissue sections with PI (Fig. 3). Neuronal death was most extensive in slices from the ASM-KO mice (Fig. 3C). WT and Het slice cultures showed similar levels of PI staining (Fig. 3A and B). Cell death units were determined by computer-based image analysis (setting mock-infected cultures to 1) (Fig. 3D). There was more cell death in the ASM-KO than in the WT and Het slice cultures ($P < 0.01$, Student's t test). The amounts of infectious virus released into the supernatant fluids of the slice cultures for the first 48 h of infection were not significantly different ($P = 0.107$, two-way ANOVA) (Fig. 3E).

Virus distribution in the cortex and hippocampus. To determine the amount and distribution of viral RNA, in situ hybridization was performed on brain sections 3 days after infection (Fig. 4). SV RNA was detected mainly in neurons in the cortex and hippocampus (Fig. 4B, D, F, H, J, and L). The

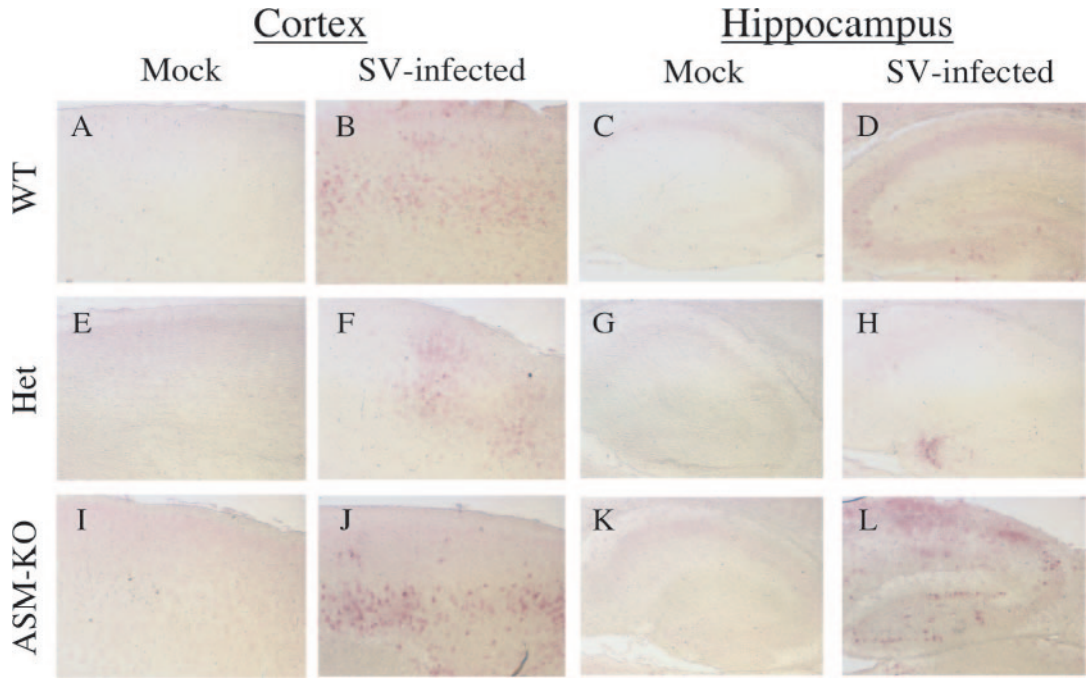

FIG. 4. SV RNA distribution in the cortex and hippocampus. In situ hybridization was performed with a DIG-labeled antisense RNA probe specific to the E2 region of SV, and SV RNA distribution was detected using anti-DIG antibody conjugated to alkaline phosphatase visualized using Fast Red. The distribution of the SV RNA 3 days after infection was more extensive in the cortex and hippocampus of ASM-KO mice (J and L) than in those of WT (B and D) and Het (F and H) mice, where only sporadic foci of infected neurons were detected. Pictures shown are representative of two independently sampled mice from each genotype. Magnification, ×100.

distributions of SV antigen in the cerebral cortex of WT and Het brains were similar, with foci of infected neurons detected throughout the region (Fig. 4B and F), but the distribution was more extensive and intense in ASM-KO mice (Fig. 4J). In the hippocampal regions of WT and Het mice, we detected a few infected neurons in the dentate gyrus and very little staining in the CA1 and CA2 regions (Fig. 4D and H). The ASM-KO mice, however, had extensive staining of SV RNA in the hippocampus, especially in the dentate gyrus and the CA1 and CA2 regions (Fig. 4L).

Immunohistochemistry was performed to determine the distribution of SV proteins within the cortex and hippocampal region (Fig. 5). Similarly to the results obtained from the in situ hybridization, the staining of SV antigen in the cortex of ASM-KO mice was more extensive and intense (Fig. 5J) than in brains from WT and Het mice (Fig. 5B and F). Extensive SV antigen was also detected in the dentate gyrus and the CA1 and CA2 regions of the hippocampus of ASM-KO mice (Fig. 5L) but not in those of WT or Het mice (Fig. 5D and H).

TUNEL staining for neuronal death in cortex and hippocampus. A TUNEL assay was used to assess the extent of cell death 3 days after infection. Mock-infected samples showed no TUNEL staining (Fig. 6A, C, E, G, I, and K). For the WT and Het brains, the staining patterns were very similar in the cerebral cortex, with only sporadic foci of TUNEL-positive neurons detected (Fig. 6B and F). More TUNEL-positive cells were present in the cerebral cortex of ASM-KO mice (Fig. 6J). For the hippocampus of WT and Het mice, TUNEL-positive cells were present only in the dentate gyrus (Fig. 6D and H). For ASM-KO mice, there was extensive TUNEL staining of the pyramidal cells of CA1 and CA2 and neurons of the dentate gyrus (Fig. 6L). Most of the TUNEL-positive cells present in the cortex and hippocampus were neurons (Fig. 6J and L) and correlated with the distribution of SV RNA and antigen in infected ASM-KO brains (Fig. 4J and L and 5J and L).

Cytokines in the brain after infection. Processing and release of cytokines are affected in ASM-KO mice (10), and increased cytokine production has been implicated in SV-induced mortality (29, 67). To investigate the potential involvement of cytokines in the accelerated death of ASM-KO mice, the levels of three cytokines involved in the innate response to CNS infection (i.e., IL-1β, TNF-α, and IL-6) were determined. Levels of IL-1β in the brain peaked at day 1, followed by a gradual decrease (Fig. 7A). Levels of IL-1β in the spinal cord increased on day 1 and then remained relatively constant (Fig. 7B). ASM-KO animals consistently had lower levels of IL-1β than WT and Het animals ($P = 0.0017$, two-way ANOVA). Levels of TNF-α in the brains and spinal cords of infected WT, Het, and ASM-KO mice were different ($P = 0.0291$ and $P = 0.0035$, two-way ANOVA) (Fig. 7C and D). Levels of TNF-α in the spinal cords of WT mice were consistently higher than those for Het and ASM-KO animals, but this could reflect differences in the basal levels of TNF-α in uninfected mice (Fig. 7D). For the brains of infected WT and Het mice, there was an initial upregulation of IL-6 on day 1, followed by a gradual decrease (Fig. 7E). For the ASM-KO brains, there was also an initial increase in IL-6 on day 1, followed by a further increase, resulting in levels three to six times higher than those of WT and Het brains ($P < 0.001$, two-way ANOVA) (Fig.

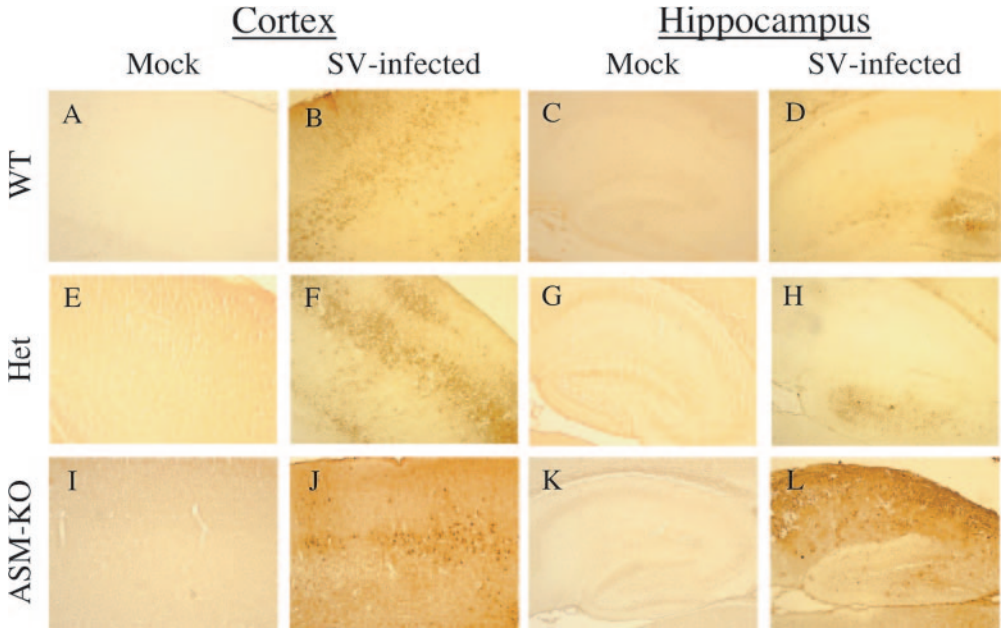

FIG. 5. SV antigen distribution in the cortex and hippocampus. Staining of SV antigen (brown) in the brains of 8-day-old WT (B and D), Het (F and H), and ASM-KO (J and L) B6 mice 3 days after infection, compared to mock-infected WT (A and C), Het (E and G), and ASM-KO (I and K) samples. The distribution of the SV antigen is more extensive in the cerebral cortex of ASM-KO mice (J) than in that of WT (B) and Het (F) mice, where only sporadic foci of infected neurons were detected. The pyramidal cells in the hippocampus of the ASM-KO mice (L) also showed extensive immunoreactivity for SV, but those of WT (D) and Het (H) mice did not. Magnification, ×100.

7E). Spinal cord IL-6 levels were similar ($P = 0.7821$, two-way ANOVA) (Fig. 7F).

Role of IL-6 in SV-induced fatal encephalomyelitis. To determine whether IL-6 has a role in the pathogenesis of SV-induced fatal encephalitis, IL-6-KO C57BL/6J mice (26) were studied (Fig. 8A). Homozygous IL-6-KO mice develop normally but fail to effectively control infection with vaccinia virus and *Listeria monocytogenes* (26). All IL-6-KO mice infected

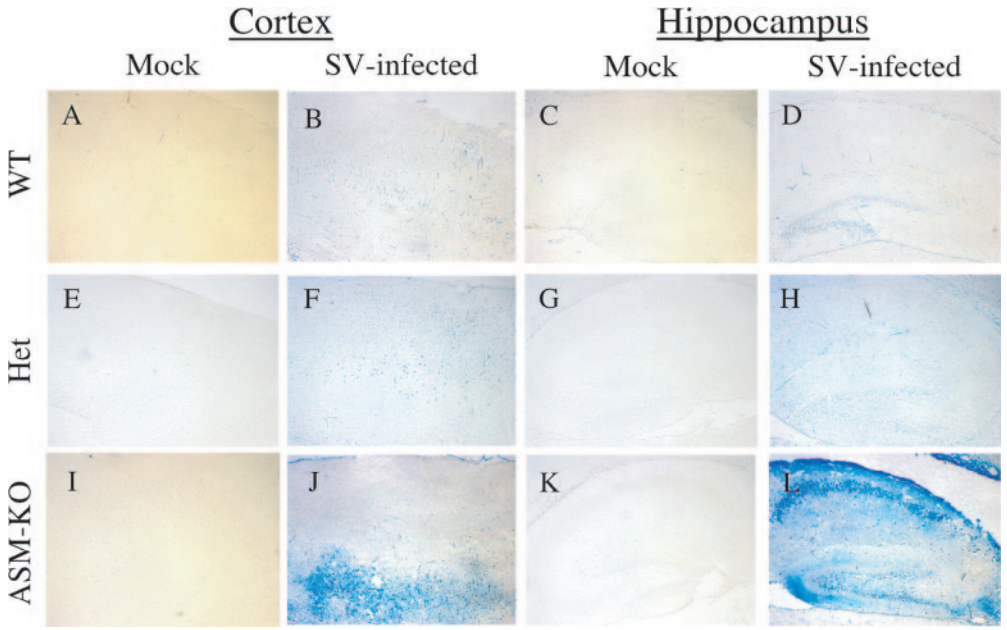

FIG. 6. TUNEL staining of the cortex and hippocampus. TUNEL staining (blue) of the brains of 8-day-old WT (B and D), Het (F and H), and ASM-KO (J and L) B6 mice 3 days after infection with SV, compared to mock-infected WT (A and C), Het (E and G), and ASM-KO (I and K) samples. More TUNEL-positive cells were present in the cerebral cortex of ASM-KO mice (J) than in that of WT (B) and Het (F) mice, where only sporadic foci of cell death were detected. The pyramidal cells and dentate gyrus in the hippocampus of the ASM-KO mice (L) also showed extensive TUNEL staining. In WT (D) or Het (H) mice, only cells in the dentate gyrus region of the hippocampus were TUNEL positive. Magnification, ×100.

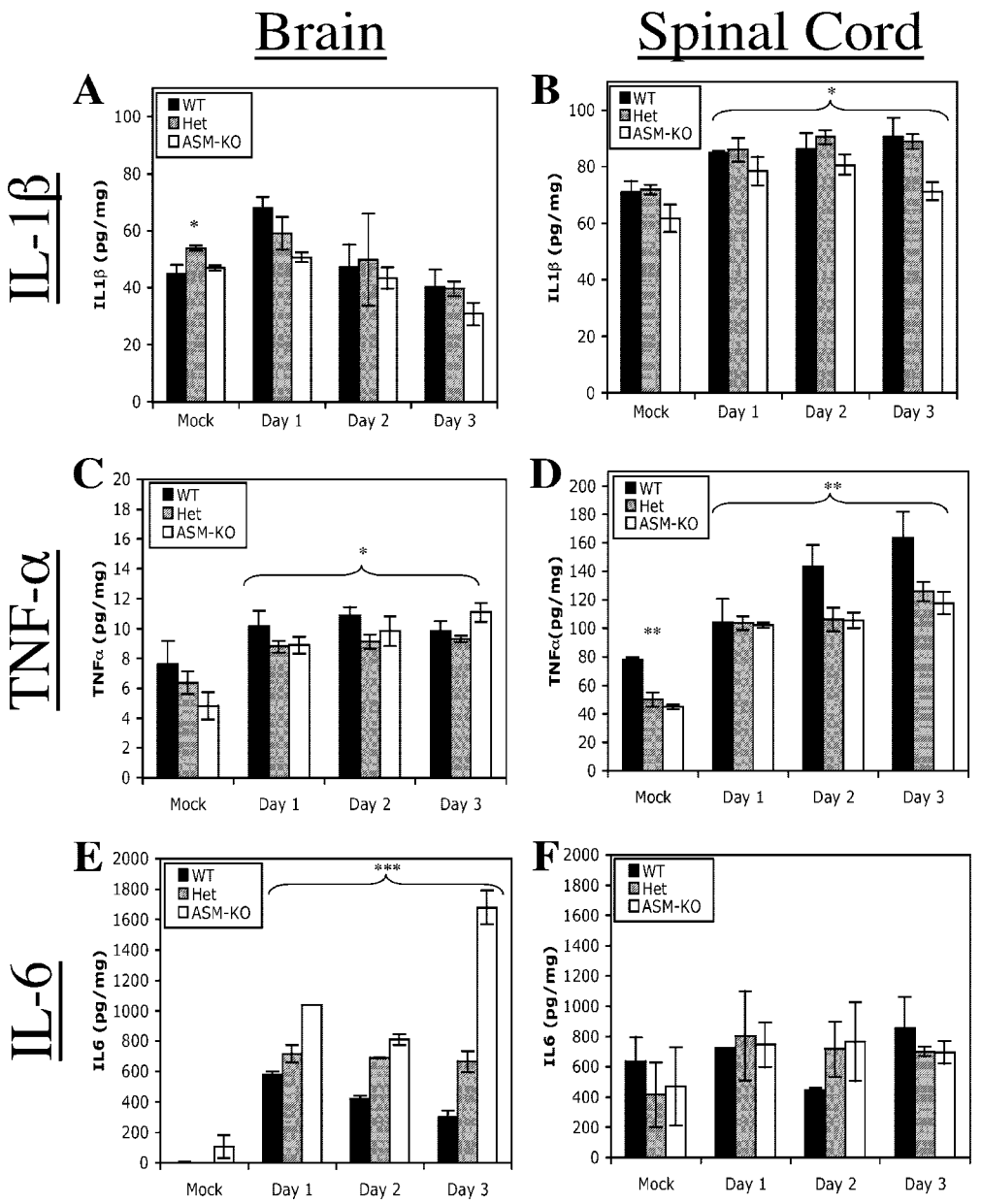

FIG. 7. Cytokine levels in the brain and spinal cord. Levels of IL-1β (A and B), TNF-α (C and D), and IL-6 (E and F) were determined by EIA in the brain (A, C, and E) and spinal cord (B, D, and F) samples collected from WT, Het, and ASM-KO mice. Infected samples were pooled ($n \geq 4$ for each time point), and the geometric means ± standard deviations of three replicates are shown (*, $P < 0.05$; **, $P < 0.005$; ***, $P < 0.001$; ANOVA).

with SV died. The mean day of death was day 4.7 for WT mice and day 5.2 for IL-6-KO mice ($P = 0.8140$, Kaplan-Meier survival analysis, log rank test), indicating that production of IL-6 per se was not responsible for more-rapid death in ASM-KO mice.

The mIL-6 gene was cloned into the dsTE SV vector in the forward and reverse orientations (dsTE-IL-6F and dsTE-IL-6R, respectively) to investigate the effects of overexpression of IL-6 on the pathogenesis of SV. Infection of BHK cells with dsTE-IL-6F showed high levels of mIL-6 expression (data not shown). dsTE-IL-6R caused 100% mortality, with the mean day of death as day 4.4, and dsTE-IL-6F caused 90% mortality, with the mean day of death as day 5.2 (Fig. 8B) ($P = 0.1030$, Kaplan-Meier survival analysis, log rank test).

DISCUSSION

In this study, we have characterized SV infection of transgenic mice deficient in the ASMase gene. ASM-KO mice were more susceptible to SV-induced fatal encephalomyelitis than WT and Het animals, and replication of SV in the brains was higher. More SV RNA, SV antigen, and TUNEL-positive neurons were present in the cortex and hippocampus of ASM-KO mice than for WT and Het mice. Hippocampal slice cultures

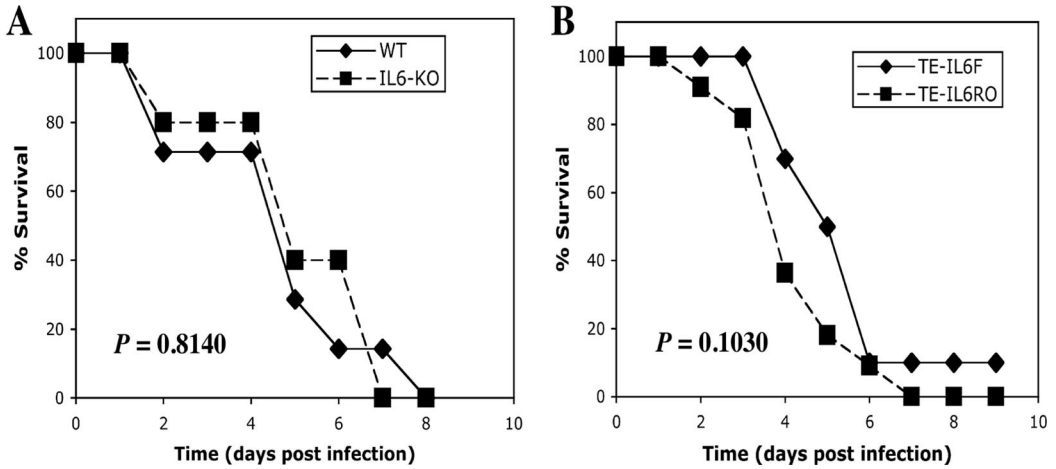

FIG. 8. Effect of IL-6 on mouse survival. (A) Eight-day-old WT ($n = 7$) and IL-6-KO ($n = 6$) mice were infected intracranially with 1,000 PFU of SV. The survival time for IL-6-KO mice after infection was similar to that for WT mice ($P = 0.8140$, Kaplan-Meier survival analysis, log rank test). (B) Eight-day-old WT mice were infected intracranially with 1,000 PFU dsTE-IL-6F ($n = 10$) and dsTE-IL-6R ($n = 11$). The survival times were similar ($P = 0.1030$, Kaplan-Meier survival analysis, log rank test).

from ASM-KO mice showed more neuronal death after infection with SV than cultures from WT or Het mice. Although IL-6 levels were higher in the brains of ASM-KO mice than in the brains of WT and Het mice 3 days after infection, studies with IL-6-KO mice and SV expressing IL-6 demonstrated that IL-6 levels per se did not affect mortality. These data indicated that the increased susceptibility of ASM-KO mice to SV-induced encephalomyelitis was the result of increased replication and more-rapid spread of SV within the CNS, which resulted in more-rapid and widespread neuronal death.

During alphavirus replication, there are multiple membrane-dependent steps that may be affected by altered lipid metabolism. ASM-KO mice have an increase in SM and a reduction of cholesterol in the plasma membrane and an accumulation of lactosylceramides in the Golgi body and smooth endoplasmic reticulum, while the lipid compositions of the RER and mitochondria are relatively unaffected (41). Cholesterol and SM are critical in mediating entry of SV into host cells (30, 56, 66), RNA synthesis takes place on the cytoplasmic surface of intracellular membranes derived from endosomes and lysosomes, and the synthesis of envelope proteins occurs at the RER (22). Electron microscopic analysis of ASM-KO mice has shown that the accumulation of SM results in formation of numerous multilamellar, cytoplasmic inclusions, particularly in the brain (17). Proliferation of intracellular smooth membranes in the brain induced by gold sodium thiomalate is associated with enhanced replication of avirulent strains of Semliki Forest virus, another alphavirus, in the brains of mature mice (37, 44). This pool of lipids in neurons of ASM-KO mice may increase availability of the intracellular membranes needed for efficient SV replication, thereby increasing viral spread.

Alterations in membrane lipid trafficking regulated by Rab GTPases (36) may also affect SV replication. For instance, the localization and function of Rab4 are perturbed by an elevation of intracellular cholesterol (4). In addition, the phenotypes of several sphingolipid storage diseases (including NPD-A, NPD-C, and GM_1 gangliosidosis) are corrected by overexpressing members of the Rab family of small GTPases (3, 34), suggesting that an elevation of sphingolipid and cholesterol within NPD-A fibroblasts results in defective intracellular targeting and trafficking of these lipids. The late-endosome-to-plasma-membrane vesicular transport pathway is important for the assembly and exit of many enveloped viruses (38), potentially including alphaviruses. However, the cellular factors that are involved in the SV assembly and release in neurons are unknown.

The importance of transsynaptic spread of alphaviruses in the CNS has been suggested in a number of studies (38, 42). There is increasing evidence that both measles and polio viruses spread between neurons primarily by cell-cell contact (6, 8, 27). The current studies suggest a more rapid and efficient transmission of SV between neurons of ASM-KO mice. This could be the result of changes in lipid composition of the plasma membrane or alterations in the exocytosis of synaptic vesicles.

In addition to effects on replication and spread, altered lipid composition may affect neuronal susceptibility to cell death. Because ceramide derived from cleavage of SM by SMase is a second messenger that can induce apoptosis (25, 45) and because SV infection activates ASMase (18), we originally hypothesized that ASMase deficiency might protect neurons from virus-induced cell death. However, increased neuronal death was present in SV-infected ASM-KO mice both in vivo and in hippocampal slice cultures even though the amount of infectious virus released by the slice cultures was not larger than that for WT or Het mice. The failure to observe the same higher virus replication in slice cultures as in brain homogenates from ASM-KO mice may be a consequence of assaying homogenates from the brains and supernatant fluids from the cultures if virus is not efficiently released from neurons into the supernatant fluid. Alternately, neurons from ASM-KO mice may be more susceptible to SV-induced cell death independent of their susceptibility to virus replication. Potential mechanisms include increased baseline levels of cellular stress associated with lipid accumulation, de-

creased activation of nitric oxide synthase (46) necessary for generation of nitric oxide, which is neuroprotective in SV encephalomyelitis (63), or need for the protective properties of ceramide-induced antioxidants (9).

The high sensitivity of the hippocampal neurons of the ASM-KO mice to SV-induced death is of particular interest. In contrast to ASMase, which is distributed in all mammalian organs, NSMase is located mostly in the CNS (15, 28, 43, 62). NSMase generation of ceramide can mediate the induction of apoptosis in hippocampal neurons by nerve growth factor and human immunodeficiency virus type 1 gp120 (1a, 19). Death-associated protein kinase, a Ca^{2+}/calmodulin-regulated serine/threonine kinase, plays a central role in ceramide-induced cell death in neurons, especially hippocampal neurons (5, 45). Previous experiments have shown an increase in NSMase activity in NPD-A fibroblasts following SV infection that was earlier and greater than that in control fibroblasts (18). We have detected an upregulation of NSMase activities in the CNSs of all three genotypes of mice investigated, suggesting that NSMase, through ceramide and death-associated protein kinase, might participate in the induction of apoptosis in the hippocampal neurons by SV.

ASMase plays a role in susceptibility to other infections. ASM-KO mice have increased susceptibility to *P. aeruginosa* because they fail to generate ceramide-enriched membrane platforms necessary for internalization of the bacteria, apoptosis, and regulation of the cytokine response, leading to a massive release of IL-1β and septic death of infected mice (10). The levels of IL-1β and TNF-α in the CNS increased with SV infection. However, ASM-KO mice did not have higher levels than WT or Het mice. Levels of IL-6, a cytokine produced by astrocytes, microglia, and neurons within the CNS (12, 21), were higher in the brains of ASM-KO mice than in the brains of WT and Het mice 3 days after infection. Overexpression of IL-6 by astrocytes results in enhanced sensitivity to glutamatergic-induced seizures and death (52). IL-6 is also upregulated in Alzheimer's disease, Parkinson's disease, strokes, encephalitis, and human immunodeficiency virus-associated dementia (2, 21, 52), suggesting a possible role in increased susceptibility of ASM-KO mice to SV infection. However, a deficiency in IL-6 did not protect mice from fatal encephalitis, and overexpression of IL-6 with a recombinant SV did not increase mortality. These data suggest that the increase in IL-6 is a response to increased virus replication rather than the cause of more-rapid death.

In summary, mice with a defect in the ASMase gene were more susceptible to SV-induced fatal encephalomyelitis due to increased replication, spread, and neuronal death. We hypothesize that this increase is associated with alterations in cellular membrane lipid composition and distribution caused by the ASMase deficiency.

ACKNOWLEDGMENTS

We thank Subroto Chatterjee for his assistance with the acid and neutral sphingomyelinase assays and Shifa Zou and Irina Shats for technical support in preparation of organotypic cultures and immunohistochemistry.

This work was supported by research grant RO1 NS18596 from the National Institutes of Health. C. G. Ng was supported by the Agency for Science, Technology and Research of Singapore.

REFERENCES

1. **Bradford, M. M.** 1976. A rapid and sensitive method for the quantitation of microgram quantities of protein utilizing the principle of protein-dye binding. Anal. Biochem. **72:**248–254.
1a. **Brann, A. B., M. Tcherpakov, I. M. Williams, A. H. Futerman, and M. Fainzilber.** 2002. Nerve growth factor-induced p75-mediated death of cultured hippocampal neurons is age-dependent and transduced through ceramide generated by neutral sphingomyelinase. J. Biol. Chem. **277:**9812–9818.
2. **Campbell, I. L., C. R. Abraham, E. Masliah, P. Kemper, J. D. Inglis, M. B. Oldstone, and L. Mucke.** 1993. Neurologic disease induced in transgenic mice by cerebral overexpression of interleukin 6. Proc. Natl. Acad. Sci. USA **90:**10061–10065.
3. **Choudhury, A., M. Dominguez, V. Puri, D. K. Sharma, K. Narita, C. L. Wheatley, D. L. Marks, and R. E. Pagano.** 2002. Rab proteins mediate Golgi transport of caveola-internalized glycosphingolipids and correct lipid trafficking in Niemann-Pick C cells. J. Clin. Investig. **109:**1541–1550.
4. **Choudhury, A., D. K. Sharma, D. L. Marks, and R. E. Pagano.** 2004. Elevated endosomal cholesterol levels in Niemann-Pick cells inhibit rab4 and perturb membrane recycling. Mol. Biol. Cell **15:**4500–4511.
5. **Cohen, O., and A. Kimchi.** 2001. DAP-kinase: from functional gene cloning to establishment of its role in apoptosis and cancer. Cell Death Differ. **8:**6–15.
6. **Daley, J. K., L. A. Gechman, J. Skipworth, and G. F. Rall.** 2005. Poliovirus replication and spread in primary neuron cultures. Virology **340:**10–20.
7. **Duan, R. D., T. Bergman, N. Xu, J. Wu, Y. Cheng, J. Duan, S. Nelander, C. Palmberg, and A. Nilsson.** 2003. Identification of human intestinal alkaline sphingomyelinase as a novel ecto-enzyme related to the nucleotide phosphodiesterase family. J. Biol. Chem. **278:**38528–38536.
8. **Firsching, R., C. J. Buchholz, U. Schneider, R. Cattaneo, V. ter Meulen, and J. Schneider-Schaulies.** 1999. Measles virus spread by cell-cell contacts: uncoupling of contact-mediated receptor (CD46) downregulation from virus uptake. J. Virol. **73:**5265–5273.
9. **Goodman, Y., and M. P. Mattson.** 1996. Ceramide protects hippocampal neurons against excitotoxic and oxidative insults, and amyloid beta-peptide toxicity. J. Neurochem. **66:**869–872.
10. **Grassme, H., V. Jendrossek, A. Riehle, G. von Kurthy, J. Berger, H. Schwarz, M. Weller, R. Kolesnick, and E. Gulbins.** 2003. Host defense against Pseudomonas aeruginosa requires ceramide-rich membrane rafts. Nat. Med. **9:**322–330.
11. **Grassme, H., A. Riehle, B. Wilker, and E. Gulbins.** 2005. Rhinoviruses infect human epithelial cells via ceramide-enriched membrane platforms. J. Biol. Chem. **280:**26256–26262.
12. **Gruol, D. L., and T. E. Nelson.** 1997. Physiological and pathological roles of interleukin-6 in the central nervous system. Mol. Neurobiol. **15:**307–339.
13. **Hannun, Y. A.** 1996. Functions of ceramide in coordinating cellular responses to stress. Science **274:**1855–1859.
14. **Higuchi, M., S. Singh, J. P. Jaffrezou, and B. B. Aggarwal.** 1996. Acidic sphingomyelinase-generated ceramide is needed but not sufficient for TNF-induced apoptosis and nuclear factor-κB activation. J. Immunol. **156:**297–304.
15. **Hofmann, K., S. Tomiuk, G. Wolff, and W. Stoffel.** 2000. Cloning and characterization of the mammalian brain-specific, Mg^{2+}-dependent neutral sphingomyelinase. Proc. Natl. Acad. Sci. USA **97:**5895–5900.
16. **Holthuis, J. C., T. Pomorski, R. J. Raggers, H. Sprong, and G. Van Meer.** 2001. The organizing potential of sphingolipids in intracellular membrane transport. Physiol. Rev. **81:**1689–1723.
17. **Horinouchi, K., S. Erlich, D. P. Perl, K. Ferlinz, C. L. Bisgaier, K. Sandhoff, R. J. Desnick, C. L. Stewart, and E. H. Schuchman.** 1995. Acid sphingomyelinase deficient mice: a model of types A and B Niemann-Pick disease. Nat. Genet. **10:**288–293.
18. **Jan, J.-T., S. B. Chatterjee, and D. E. Griffin.** 2000. Sindbis virus entry into cells triggers apoptosis by activating sphingomyelinase, leading to the release of ceramide. J. Virol. **74:**6425–6432.
19. **Jana, A., and K. Pahan.** 2004. Human immunodeficiency virus type 1 gp120 induces apoptosis in human primary neurons through redox-regulated activation of neutral sphingomyelinase. J. Neurosci. **24:**9531–9540.
20. **Johnson, R. T., H. F. McFarland, and S. E. Levy.** 1972. Age-dependent resistance to viral encephalitis: studies of infections due to Sindbis virus in mice. J. Infect. Dis. **125:**257–262.
21. **Juttler, E., V. Tarabin, and M. Schwaninger.** 2002. Interleukin-6 (IL-6): a possible neuromodulator induced by neuronal activity. Neuroscientist **8:**268–275.
22. **Kielian, M.** 1995. Membrane fusion and the alphavirus life cycle. Adv. Virus Res. **45:**113–151.
23. **Kimura, T., and D. Griffin.** 2003. Extensive immune-mediated hippocampal damage in mice surviving infection with neuroadapted Sindbis virus. Virology **311:**28–39.
24. **Kolesnick, R.** 2002. The therapeutic potential of modulating the ceramide/sphingomyelin pathway. J. Clin. Investig. **110:**3–8.

25. **Kolesnick, R. N., and M. Kronke.** 1998. Regulation of ceramide production and apoptosis. Annu. Rev. Physiol. **60:**643–665.
26. **Kopf, M., H. Baumann, G. Freer, M. Freudenberg, M. Lamers, T. Kishimoto, R. Zinkernagel, H. Bluethmann, and G. Kohler.** 1994. Impaired immune and acute-phase responses in interleukin-6-deficient mice. Nature **368:**339–342.
27. **Lawrence, D. M., C. E. Patterson, T. L. Gales, J. L. D'Orazio, M. M. Vaughn, and G. F. Rall.** 2000. Measles virus spread between neurons requires cell contact but not CD46 expression, syncytium formation, or extracellular virus production. J. Virol. **74:**1908–1918.
28. **Levade, T., R. Salvayre, and L. Douste-Blazy.** 1986. Sphingomyelinases and Niemann-Pick disease. J. Clin. Chem. Clin. Biochem. **24:**205–220.
29. **Liang, X.-H., J. E. Goldman, H. H. Jiang, and B. Levine.** 1999. Resistance of interleukin-1β-deficient mice to fatal Sindbis virus encephalitis. J. Virol. **73:**2563–2567.
30. **Lu, Y. E., T. Cassese, and M. Kielian.** 1999. The cholesterol requirement for Sindbis virus entry and exit and characterization of a spike protein region involved in cholesterol dependence. J. Virol. **73:**4272–4278.
31. **Lu, Y. E., and M. Kielian.** 2000. Semliki Forest virus budding: assay, mechanisms, and cholesterol requirement. J. Virol. **74:**7708–7719.
32. **Lustig, S., A. C. Jackson, C. S. Hahn, D. E. Griffin, E. G. Strauss, and J. H. Strauss.** 1988. The molecular basis of Sindbis virus neurovirulence in mice. J. Virol. **62:**2329–2336.
33. **Marchesini, N., and Y. A. Hannun.** 2004. Acid and neutral sphingomyelinases: roles and mechanisms of regulation. Biochem. Cell Biol. **82:**27–44.
34. **Marks, D. L., and R. E. Pagano.** 2002. Endocytosis and sorting of glycosphingolipids in sphingolipid storage disease. Trends Cell Biol. **12:**605–613.
35. **Marquardt, M. T., T. Phalen, and M. Kielian.** 1993. Cholesterol is required in the exit pathway of Semliki Forest virus. J. Cell Biol. **123:**57–65.
36. **Martinez, O., and B. Goud.** 1998. Rab proteins. Biochim. Biophys. Acta **1404:**101–112.
37. **Mehta, S., S. Pathak, and H. E. Webb.** 1990. Induction of membrane proliferation in mouse CNS by gold sodium thiomalate with reference to increased virulence of the avirulent Semliki Forest virus. Biosci. Rep. **10:**271–279.
38. **Murray, J. L., M. Mavrakis, N. J. McDonald, M. Yilla, J. Sheng, W. J. Bellini, L. Zhao, J. M. Le Doux, M. W. Shaw, C. C. Luo, J. Lippincott-Schwartz, A. Sanchez, D. H. Rubin, and T. W. Hodge.** 2005. Rab9 GTPase is required for replication of human immunodeficiency virus type 1, filoviruses, and measles virus. J. Virol. **79:**11742–11751.
39. **Nieva, J.-L., R. Bron, J. Corver, and J. Wilschut.** 1994. Membrane fusion of Semliki Forest virus requires sphingolipids in the target membrane. EMBO J. **13:**2797–2804.
40. **Nilsson, A., and R. D. Duan.** 1999. Alkaline sphingomyelinases and ceramidases of the gastrointestinal tract. Chem. Phys. Lipids **102:**97–105.
41. **Nix, M., and W. Stoffel.** 2000. Perturbation of membrane microdomains reduces mitogenic signaling and increases susceptibility to apoptosis after T cell receptor stimulation. Cell Death Differ. **7:**413–424.
42. **Oliver, K. R., and J. K. Fazakerley.** 1998. Transneuronal spread of Semliki Forest virus in the developing mouse olfactory system is determined by neuronal maturity. Neuroscience **82:**867–877.
43. **Otterbach, B., and W. Stoffel.** 1995. Acid sphingomyelinase-deficient mice mimic the neurovisceral form of human lysosomal storage disease (Niemann-Pick disease). Cell **81:**1053–1061.
44. **Pathak, S., S. J. Illavia, and H. E. Webb.** 1983. The identification and role of cells involved in CNS demyelination in mice after Semliki Forest virus infection: an ultrastructural study. Prog. Brain Res. **59:**237–254.
45. **Pelled, D., T. Raveh, C. Riebeling, M. Fridkin, H. Berissi, A. H. Futerman, and A. Kimchi.** 2002. Death-associated protein (DAP) kinase plays a central role in ceramide-induced apoptosis in cultured hippocampal neurons. J. Biol. Chem. **277:**1957–1961.
46. **Perrotta, C., C. De Palma, S. Falcone, C. Sciorati, and E. Clementi.** 2005. Nitric oxide, ceramide and sphingomyelinase-coupled receptors: a tale of enzymes and messengers coordinating cell death, survival and differentiation. Life Sci. **77:**1732–1739.
47. **Peterson, K. E., J. S. Errett, T. Wei, D. E. Dimcheff, R. Ransohoff, W. A. Kuziel, L. Evans, and B. Chesebro.** 2004. MCP-1 and CCR2 contribute to non-lymphocyte-mediated brain disease induced by Fr98 polytropic retrovirus infection in mice: role for astrocytes in retroviral neuropathogenesis. J. Virol. **78:**6449–6458.
48. **Pollak, Y., A. Gilboa, O. Ben Menachem, T. Ben Hur, H. Soreq, and R. Yirmiya.** 2005. Acetylcholinesterase inhibitors reduce brain and blood interleukin-1beta production. Ann. Neurol. **57:**741–745.
49. **Quintern, L. E., and K. Sandhoff.** 1991. Human acid sphingomyelinase from human urine. Methods Enzymol. **197:**536–540.
50. **Ramstedt, B., and J. P. Slotte.** 2002. Membrane properties of sphingomyelins. FEBS Lett. **531:**33–37.
51. **Ruvolo, P. P.** 2003. Intracellular signal transduction pathways activated by ceramide and its metabolites. Pharmacol. Res. **47:**383–392.
52. **Samland, H., S. Huitron-Resendiz, E. Masliah, J. Criado, S. J. Henriksen, and I. L. Campbell.** 2003. Profound increase in sensitivity to glutamatergic- but not cholinergic agonist-induced seizures in transgenic mice with astrocyte production of IL-6. J. Neurosci. Res. **73:**176–187.
53. **Simons, K., and R. Ehehalt.** 2002. Cholesterol, lipid rafts, and disease. J. Clin. Investig. **110:**597–603.
54. **Simons, K., and E. Ikonen.** 1997. Functional rafts in cell membranes. Nature **387:**569–572.
55. **Sims, K. J., S. D. Spassieva, E. O. Voit, and L. M. Obeid.** 2004. Yeast sphingolipid metabolism: clues and connections. Biochem. Cell Biol. **82:**45–61.
56. **Smit, J. M., R. Bittman, and J. Wilschut.** 1999. Low-pH-dependent fusion of Sindbis virus with receptor-free cholesterol and sphingolipid-containing liposomes. J. Virol. **73:**8476–8484.
57. **Steinhart, W. L., J. S. Busch, J. P. Oettgen, and J. L. Howland.** 1984. Sphingolipid metabolism during infection of human fibroblasts by herpes simplex virus type 1. Intervirology **21:**70–76.
58. **Stoffel, W.** 1999. Functional analysis of acid and neutral sphingomyelinases in vitro and in vivo. Chem. Phys. Lipids **102:**107–121.
59. **Stoffel, W., B. Jenke, B. Block, M. Zumbansen, and J. Koebke.** 2005. Neutral sphingomyelinase 2 (smpd3) in the control of postnatal growth and development. Proc. Natl. Acad. Sci. USA **102:**4554–4559.
60. **Strauss, J. H., and E. G. Strauss.** 1994. The alphaviruses: gene expression, replication and evolution. Microbiol. Rev. **58:**491–562.
61. **Thach, D. C., T. Kimura, and D. E. Griffin.** 2000. Differences between C57BL/6 and BALB/cBy mice in mortality and virus replication after intranasal infection with neuroadapted Sindbis virus. J. Virol. **74:**6156–6161.
62. **Tomiuk, S., K. Hofmann, M. Nix, M. Zumbansen, and W. Stoffel.** 1998. Cloned mammalian neutral sphingomyelinase: functions in sphingolipid signaling? Proc. Natl. Acad. Sci. USA **95:**3638–3643.
63. **Tucker, P. C., D. E. Griffin, S. Choi, N. Bui, and S. Wesselingh.** 1996. Inhibition of nitric oxide synthesis increases mortality in Sindbis virus encephalitis. J. Virol. **70:**3972–3977.
64. **Utermohlen, O., U. Karow, J. Lohler, and M. Kronke.** 2003. Severe impairment in early host defense against Listeria monocytogenes in mice deficient in acid sphingomyelinase. J. Immunol. **170:**2621–2628.
65. **Vornov, J. J., R. C. Tasker, and J. Park.** 1995. Neurotoxicity of acute glutamate transport blockade depends on coactivation of both NMDA and AMPA/kainate receptors in organotypic hippocampal cultures. Exp. Neurol. **133:**7–17.
66. **Waarts, B. L., R. Bittman, and J. Wilschut.** 2002. Sphingolipid and cholesterol dependence of alphavirus membrane fusion. Lack of correlation with lipid raft formation in target liposomes. J. Biol. Chem. **277:**38141–38147.
67. **Wesselingh, S. L., B. Levine, R. J. Fox, S. Choi, and D. E. Griffin.** 1994. Intracerebral cytokine mRNA expression during fatal and nonfatal alphavirus encephalitis suggests a predominant type 2 T cell response. J. Immunol. **152:**1289–1297.
68. **Zumbansen, M., and W. Stoffel.** 2002. Neutral sphingomyelinase 1 deficiency in the mouse causes no lipid storage disease. Mol. Cell. Biol. **22:**3633–3638.